33RD CONGRESS
OF THE INTERNATIONAL COUNCIL
OF THE AERONAUTICAL SCIENCES
STOCKHOLM, SWEDEN, 4-9 SEPTEMBER, 2022

ICAS 2022 SWEDEN

A PRELIMINARY STRUCTURAL DESIGN OF A FLEXIBLE FLYING DEMONSTRATOR

Pedro J. González[1], Gerrit Stavorinus[2], Hikmat Shahi[3], Yasser M. Meddaikar[4], Sunpeth Cumnuantip [5], Arne Voß[6], Thomas Klimmek[7], Wolf R. Krüger[8] & Flávio J. Silvestre[9]

[1,2,3,9]Department of Flight Mechanics, Flight Control and Aeroelasticity, , Technical University of Berlin, 10587 Berlin, Germany
[4,5,6,7,8]Institute of Aeroelasticity, German Aerospace Center (DLR), Göttingen, 37073, Germany

Abstract

The objective of this paper is to present the preliminary structural design procedure of a flexible aircraft demonstrator called TU-Flex. This vehicle is designed to gather coupled flight and structural dynamics data to validate flexible aircraft models. Due to its unconventional requirements, it was necessary to use numerical methods already in the conceptual and preliminary structural design phases. This paper describes the different procedures to design the fuselage, empennage, and wings. A fast FEM generator procedure was developed for the design of the fuselage structure. It was created using OpenVSP, HyperMesh, and CAD programs. The wing structure was optimized for minimum structural weight subjected to maximum deflection and torsion constraints and it is capable to withhold all the required maneuver load cases. The wing was designed using the DLR's ModGen/NASTRAN design process. A detailed description of the finite element and aerodynamic model is given. The fully flexible model was assembled to perform a complete load analysis on the whole aircraft. The DLR's toolbox Loads Kernel is used for the load analysis of the free-flying aircraft. The model is capable of carrying different monitoring stations that allow the evaluation of forces and moments for different load cases in all desired locations of the structure. The loads analysis shows that the presented configuration is within the bounds of allowable strains and deformations and can proceed to detailed design.

Keywords: flexible aircraft design, aeroelastic structures design, flying demonstrator, aeroelasticity.

1. Introduction

In the last decades there has been a growing interest in the reduction of environmental impact of the aircraft industry. One of the solutions proposed to reduce it is to increase the aspect ratio of the wing. High aspect ratio wings increase aerodynamic efficiency and therefore reduce fuel consumption and carbon emissions. However, the development of these kinds of wings brings new challenges to structural and flight dynamics modeling. The increase of aspect ratio while keeping structural efficiency generates a reduction of the frequencies of the aeroelastic modes. These low structural modes tend to couple with flight dynamics modes of the aircraft [1]. As a consequence, the flight dynamics, handling qualities, and performance characteristics of the aircraft change with respect to the rigid body approximation, making it no longer valid [2], [3].

To date, there are several approaches to model flight dynamics of flexible aircraft depending on their level of flexibility. Nevertheless, there is not much available data for model validation of flexible aircraft (FA) [3]. Several low cost airframes have been developed to collect aerodynamic, flight dynamics and aeroelastic coupled response. The three main examples of these platforms are the mAEWing, FLEXOP and X-HALE . The mAEWing is the flutter-suppression test-bed vehicle constructed by the University of Minnesota. It was designed to research modelling techniques of flexible aircraft, as well as to study body-freedom flutter and control it [4]. The FLEXOP was built as a platform for flutter-suppression-control research, model validation and aeroelastic design. Nevertheless, the structural modes are still too high in frequency to couple with flight dynamics modes [5]. The X-HALE is a flying testbed that represents a High Altitude Long Endurance Aircraft (HALE). It was designed and

Figure 1 – mAEWing, FLEXOP and X-HALE demonstrators (clockwise from top left)

built by the University of Michigan to collect in-flight rigid body and structural dynamics data for the validation of flexible aircraft models [6]. In 2017, a version of the X-HALE was also built at the ITA in Brazil where different control techniques were tested and validated [3], [7]. Even though the flight modes are coupled with the structural dynamics in certain flight conditions, the characteristics and performance of the vehicle differ when compared to a regular transport or commercial airliner. Therefore, currently, there is a lack of flying platforms with similar configurations to commercial or transport aircraft with the capability of providing coupled structural and flight dynamic data.

In view of this situation, the TU Berlin's Department of Flight Mechanics, Flight Control and Aeroelasticity in cooperation with the German Aerospace Center's Institute of Aeroelasticity has been developing the TU-Flex. TU-Flex is a flexible testbed with a configuration that permits to trace conclusions applicable to a new generation of more efficient and eco-friendly transport and commercial airliners. The first version of the aircraft should have two sets of wings. The first set consists of a baseline configuration that allows moderate wingtip displacements around 10% with respect to the span during excitation maneuvers. The second set of wings will be classified as a very flexible wing. It should be capable to display coupling between rigid-body and structural dynamics during flight and at the same time its wingtip deflections can go near 20% with respect the half-span. This flying demonstrator will allow for the analysis and further understanding of the consequences of increased flexibility to aircraft's flight dynamics and control.

1.1 Conceptual Design Considerations and Requirements

The main difference in the conceptual design of this vehicle with respect to conventional industrial processes is the consideration of the structural flexibility at the early design stages. The conceptual requirements of TU-Flex are summarized in Table 1.
All these dimensions, especially the wing span, were established considering the fact that the aircraft must fit in the installations of the TU Berlin laboratories and SWG-DLR wind tunnel. The aircraft will also use a combination of rigid body and structural dynamics sensors to measure the shape deformation during flight. These sensors will allow the implementation of a novel control architecture that will enable the operation of the aircraft. The same sensors will permit the implementation of aeroelastic system-identification. The conceptual design of TU-Flex is shown in Fig. 2. The aircraft was designed as a T-tail configuration. This is commonly used in different transport aircraft and it allows to remove the motors from the wings, reducing the level of uncertainties in the modeling process. The fuselage was designed to store all the instrumentation needed to operate the aircraft and the retractable landing gear. In order to reduce the operational risk, the environmental impact of the demonstrator and the model uncertainty pertaining fuel consumption, the aircraft has two ducted-fan electric motors as a propulsion system.

Table 1 – TU-Flex conceptual requirements.

Wing span [m]	Max. 3.6 (semi span = 1.8 limited by wind-tunnel dimensions)
Length [m]	Max. 3
Max. wing tip deflection (2g load case)	10%(FA), 20%(VFA)
Aspect ratio	13-20
Sweep [deg]	20-28
Weight [Kg]	Max. 25
Airspeed [m/s]	20-45
Load factor range	-2.0 to 4.0
Propulsion	2x Ducted fan electric-motors
Landing Gear	Tricycle retractable
Rigid-body sensors	IMU, GPS, Pitot Probe, AoA-SSA measurements
Structural Sensors	At least 3 pairs of IMUs per wing

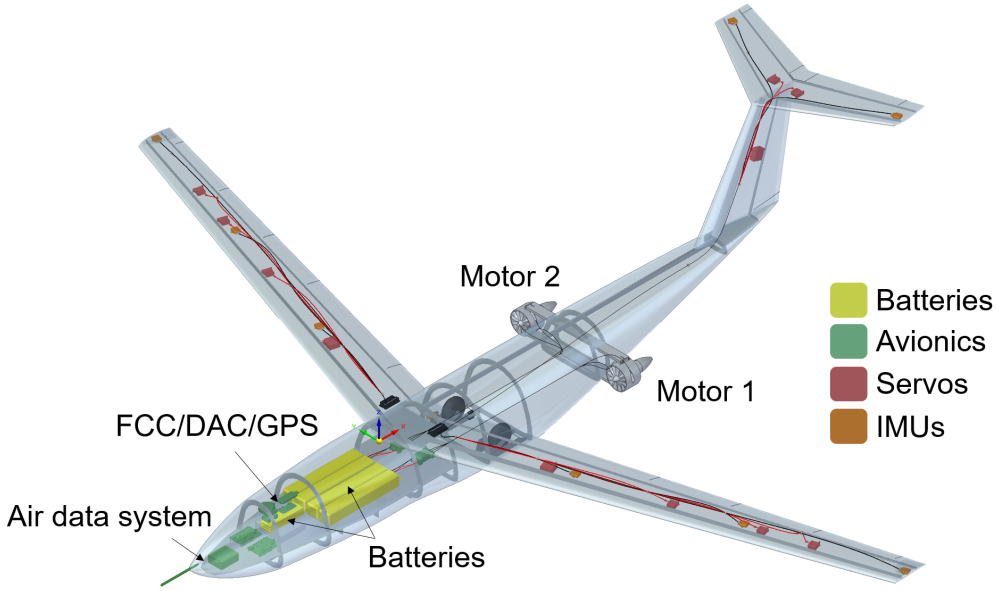

Figure 2 – TU-FLEX´s systems distribution

1.2 Objective

The objective of the work herein is to show the procedure for the preliminary design of the TU-Flex's structure. This study is focused only on the baseline wing, which is considered as a flexible wing and does not include the very flexible one. The paper shows the different procedures to generate the mesh, design the structure and evaluate the different load cases to perform the full flexible aircraft in-flight loads analysis.

2. TU-Flex's Structural Topology and Finite Element Model

The TU-Flex topology was selected based on previous experiences in the DLR's Institute of Aeroelasticity and other flying platforms such as the T2, IEP and FLEXOP [5], [8], [9], [10]. Figure 3 shows the current airframe of TU-Flex. The outer skin of the fuselage is made from a sandwich composite comprising of glass fiber composite plies and lightweight foam (ROHACELL®) with a total wall thickness of around 2.5 mm. This material composition was chosen due to its combination of high bending stiffness and low weight [8]. Attached to the outer skin are ten frames (numbered 1 to 10 from nose to tail) as well as a single longitudinal support beam running from frame 4 at the rear wing spar to frame 9 located at the front spar of the vertical stabilizer. The frames and support beam are made from the same composite laminate as the skin of the fuselage. The floor in the front half of the

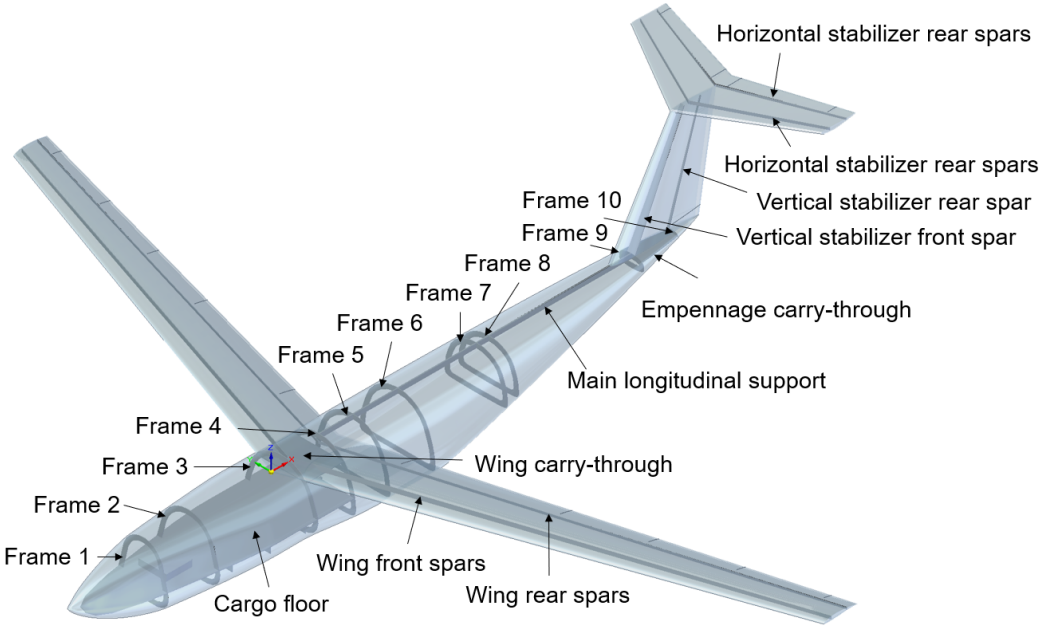

Figure 3 – TU-Flex structural concept

fuselage running from the nose to the plane to frame 4 adds stiffness to the fuselage structure and acts as the location for installing most of the internal systems. To prevent bending under the weight of the systems, the floor was reinforced on the underside with ribs as well as a support beam between the rear edge of the floor and frame 4. The front landing gear is mounted in between frame 1 and 2, the main landing gear in between frames 5 and 6. The two ducted fan motors used for propulsion are mounted to the fuselage in between frames 7 and 8.

The skin of the vertical stabilizer is made from the same material as the fuselage. The wing and stabilizer skins are supported by two spars each and are filled with lightweight foam (not pictured) to prevent buckling. The wing is designed as an enclosed shell comprising of an upper and lower skin running up to the leading and trailing edge. With the foam providing the necessary stability against buckling, ribs are not present on the wings. The wings are attached to the fuselage internally by connecting the support spars to the carry-through. This connection is detachable to allow the flexible and very flexible wing to be exchanged easily. The tail assembly is attached to the fuselage at the rear carry-through positioned between frames 9 and 10.
Figure 4 shows a flowchart of the fuselage design process. The initial model of TU-Flex was created in OpenVSP [11]. OpenVSP is an open source parametric aircraft geometry tool developed by NASA that is used in the design and creation of 3D models of aircraft. It allows the generation of preliminary aerodynamic and structural geometries for different analyses. The model of TU-Flex generated in OpenVSP only displays the basic outer geometry of the plane, so a detailed CAD model was necessary to enable designing the internal structure of the airplane.
OpenVSP allows the export of the fuselage, wing and tail assembly geometries as .stp files. These CAD models exported from OpenVSP are solid bodies, so for a realistic model the geometries have been edited in Blender [12], a 3D computer graphics software, which was used to generate hollow structures before importing them into the CAD program. Since the fuselage does not have a circular cross section, the frames were created from two-dimensional slices of the fuselage geometry which also can be exported from OpenVSP. These slices are imported into a CAD program and are then extruded and edited further. The cargo floor was created using a similar process. Additional internal structures such as the spars, the main stringer and the carry-throughs have simple rectangular geometries and were created manually with the necessary measurements being taken from the CAD model. This CAD model enabled accurate mass and center of gravity calculations, and was used to decide the internal positioning of the hardware. The model was also used as a starting point in the

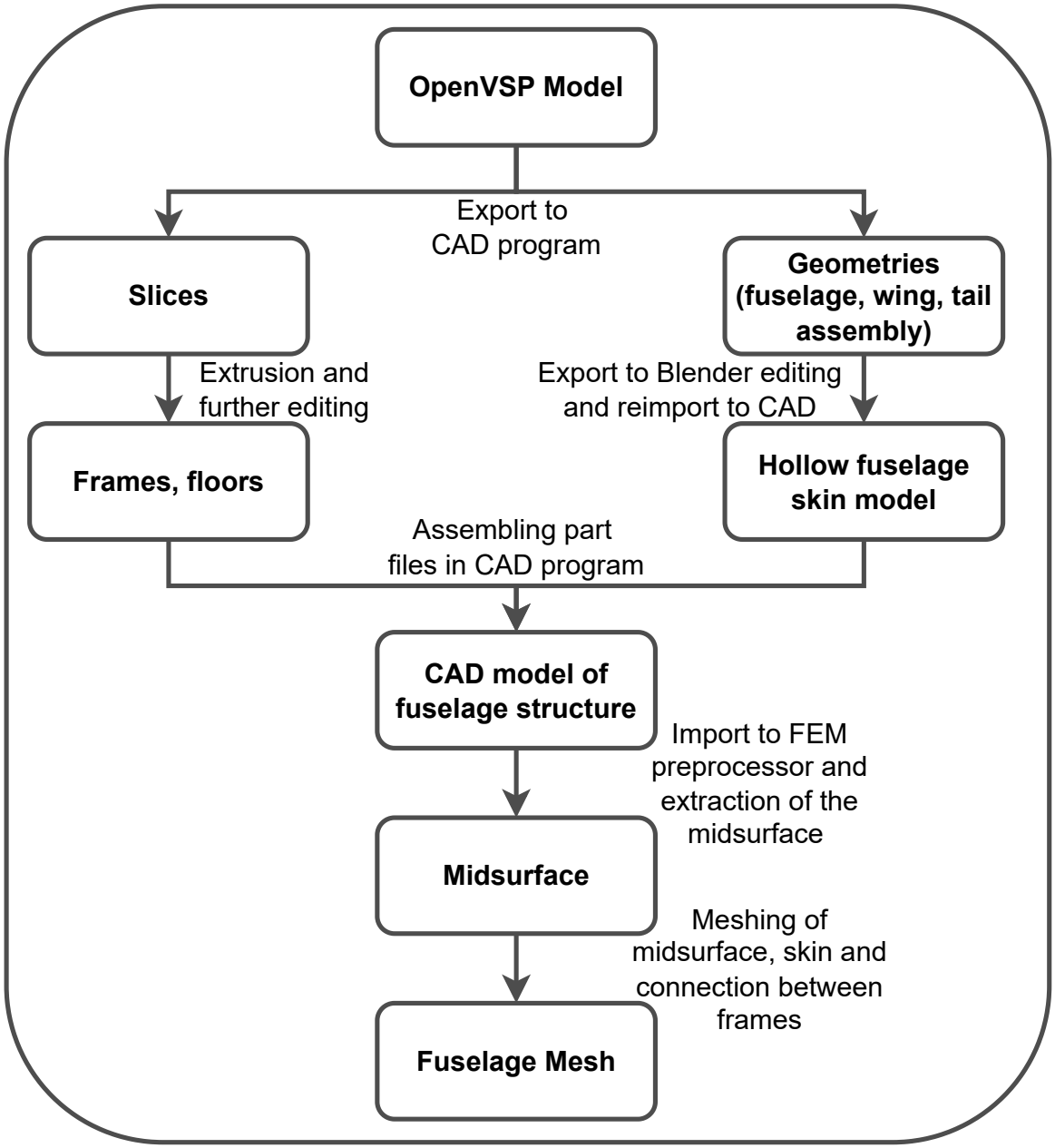

Figure 4 – Workflow of the fuselage design process

creation of the finite element mesh necessary for structural analyses. The FE-model of the fuselage and tail assembly was created in Altair HyperMesh [13], a finite element pre-processor compatible with NASTRAN that allows for easy creation of finite element meshes in a CAD like environment. In the first step the CAD model of the outer skin of the fuselage was imported into HyperMesh. HyperMesh allows the calculation of the midsurface from thin walled geometries. This midsurface was then discretized into 1650 grid points. To prevent potential computational issues the nose and rear of the fuselage were cut off. The fuselage could then be modeled with shell elements and assigned material properties. The tail assembly was created without the use of the midsurface, with relevant measurements such as leading and trailing edge coordinates, chord lengths, thicknesses, location relative to the fuselage, etc. being acquired from measurements in the CAD model and the definitions of the airfoils. The frames, floors, carry-throughs, stringer and spars, all being made from the same material as the fuselage skin, are also modeled with composite shell elements. Each frame was discretized into 16 elements. The internal systems and the two fans attached to the fuselage are modeled as mass point elements which are connected to the rest of the structure. The foam filling the wings and tail assembly is modeled with solid elements with isotropic material properties. The landing gear and

support beam are modeled as beam elements. The structural FE model of the wings and the aerodynamics DLM were generated using the in-house software ModGen [14],[15] at the DLR - Institute of Aeroelasticity. ModGen is a program aimed at generating structural finite element and aerodynamic models of wing- or fuselage-like aircraft components compatible with MSC.NASTRAN, suited for GFEM/Dynamic and aeroelastic analyses. ModGen uses parametric input files from which the desired model can be generated. It also allows for the generation of structural optimization (SOL200) or aeroelastic analysis (SOL144) input cards to be used with the generated model. The FE models of the fuselage and wing were merged in HyperMesh to create a structural model of the entire aircraft. The load maneuver case limits shown in Table 1 were used for the structural sizing. The wing's design procedure is shown in Fig. 5. The outer skin of the wings is made from a glass fibre composite laminate, with the skin thickness varying from about 1 mm at the root to about 0.1 mm at the wing tips. The wing consists of an upper and lower skin forming a shell up to the leading and trailing edge. Two spars are present aiding in an attachment to the fuselage (Fig.3). The wing is also filled with the foam core in the hollow between the upper and lower skin halves to counter buckling. The wing design was obtained based on a design study presented in [16]. The objective of the design optimization was to maximize the tip displacement of the 1g cruise condition, subjected to a tip twist constraint and the maximum strain allowed by the material. The workflow described in Fig. 5 was repeated for different design studies until the design requirements were attained.

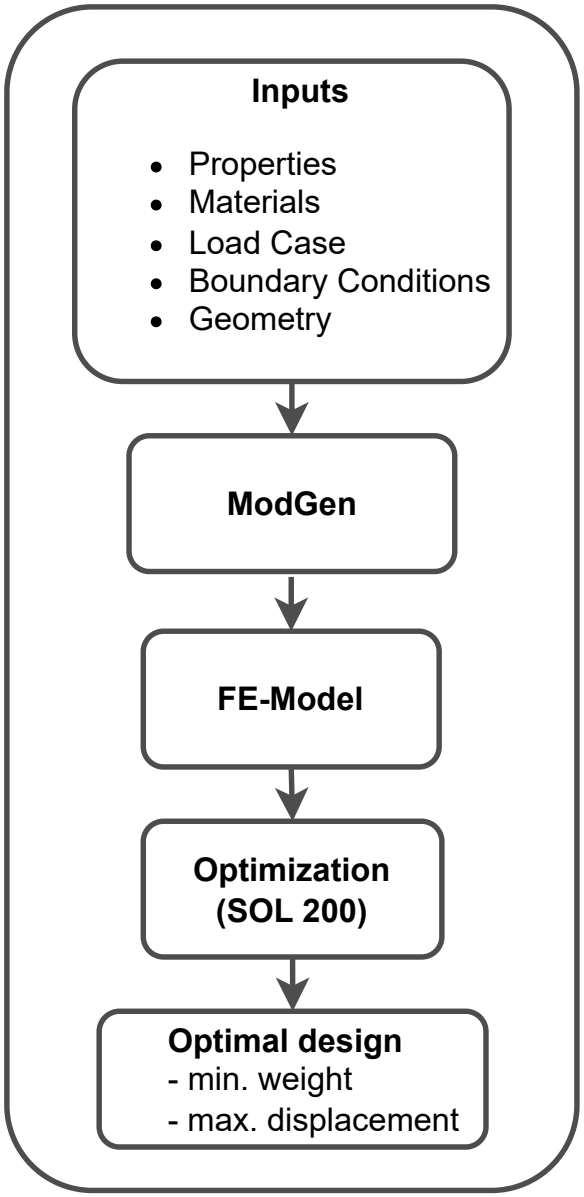

Figure 5 – Workflow of the wing design process

Figure 6 shows the FE model of TU-Flex aircraft. MSC.NASTRAN was used as the FE solver. Most of the structure of the UAV is made up of thin walled composite laminate, so shell elements (CQUAD4 and CTRIA3) are the most common type of FE element used. The foam filling of the wing and tail assembly is modeled with solid elements (CHEXA and CPENTA). The landing gear and the support beam between the floor and frame 4 are modeled with beam elements (CBEAM). The internal systems and the two ducted fan motors were modeled as concentrated mass elements (CONM2), assigned to grid points at their center of gravity. They were connected to the rest of the structure with interpolation elements (RBE3). Altogether, the model contains approximately 36,000 degrees of freedom.

Figure 7 shows the aerodynamic panel mesh for the VLM and DLM of TU-Flex. The wing, horizontal and vertail tailplane are represented as flat panels (CAERO1 and AESURF) that are discretized to form the panel model. Additional terms that serve as a correction to account for camber and twist of the profile are also present. The panel mesh for the full aircraft contains 1195 panels.

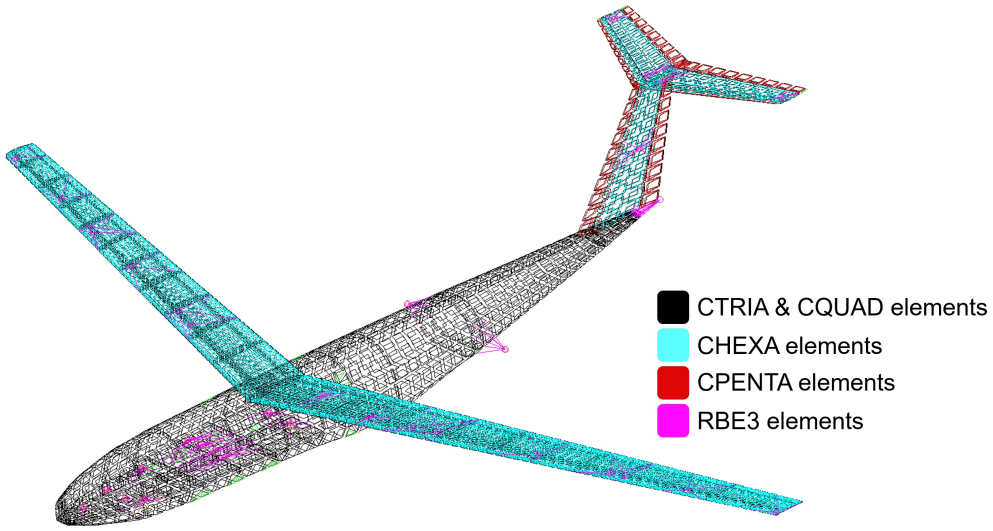

Figure 6 – TU-Flex finite element structural model

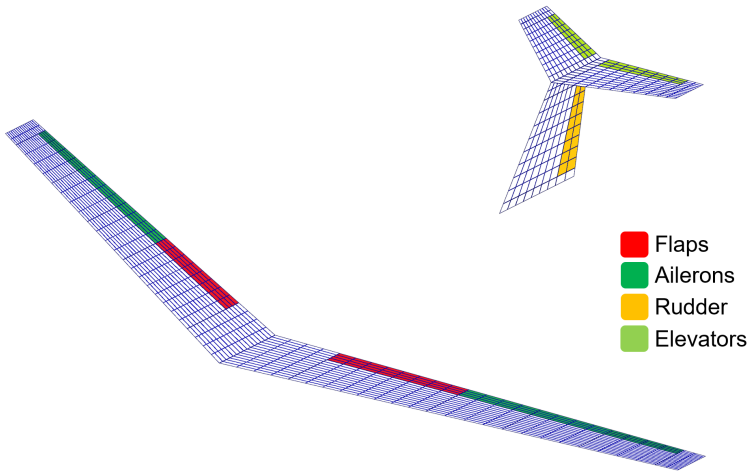

Figure 7 – TU-Flex panel mesh aerodynamic model, control surfaces highlighted

3. Full Aircraft Load Analysis

The load analysis of TU-Flex is carried out with the DLR in-house software Loads Kernel [17]. The software is a loads analysis program that couples the aerodynamic and structural models to analyse aircraft. It allows the evaluation of different trim conditions, maneuvers and load cases including unsteady gust loads as well as dynamic landing loads. The output of the program are the resulting loads on the structure. Different monitoring stations can be installed on the structure to measure the load in the desired zones of interest. Additionally to the aerodynamic and structural meshes the mass and stiffness matrices of the structure (for example obtained from MSC.NASTRAN via a DMAP alter) are required to perform a modal analysis, as the deformation of the structure under the aerodynamic forces is calculated via a modal superposition approach. Figure 8 shows the combined structural and aerodynamic models including the masses of all the aircraft systems.

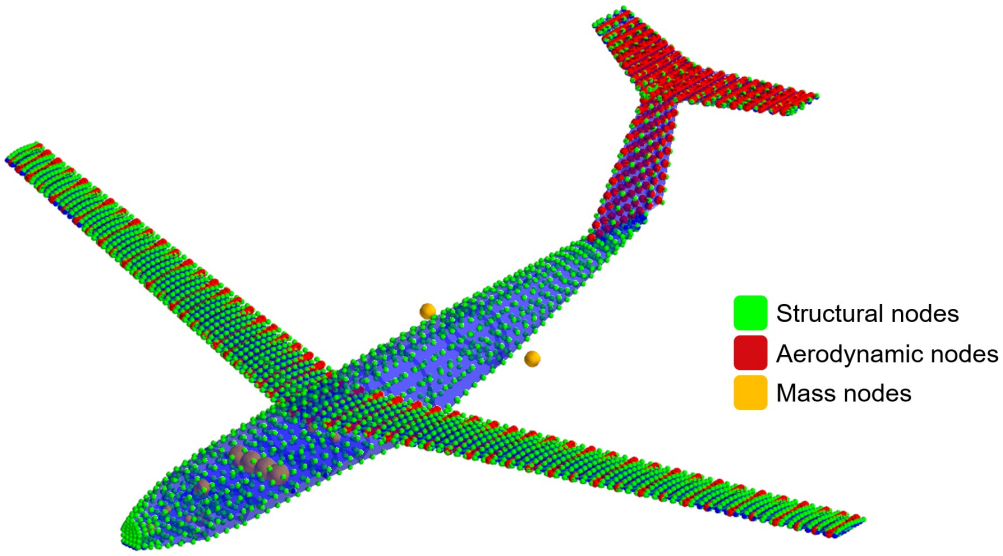

Figure 8 – Combined aeroelastic models (structure, mass, aerodynamics)

For the aero-structural coupling the aerodynamic and structural nodes of the models are associated to each other via a nearest neighbor algorithm, although spline functions defined beforehand can also be used. A transformation matrix is used to transfer forces from the aerodynamic grid to the structural grid. Loads Kernel allows modelling the aerodynamics using vortex lattice method (VLM) or doublet lattice method (DLM)[18]. The aerodynamics models are based on formulations by Katz and Plotkin [19] and Albano and Rodden [20], respectively. The steady aerodynamic forces during a maneuver are calculated with the dynamic pressure, the aerodynamic integration matrix, the aerodynamic influence coefficient matrix and the downwash at each panel. The nodal loads in the structural grid can then be calculated.
The load cases for evaluation are defined in an additional input file. With the given data Loads Kernel performs a trim calculation for each specified maneuver which results in the deformation and loads acting on the structure for the trim case.
The calculated nodal loads are integrated at monitoring stations to obtain the resulting section forces or moments. These monitoring stations are located at interesting locations of the geometry, for example at the landing gear frames, the wing root, or along the wing to analyse different loads per section. An analysis can run through several hundred load cases, including different maneuvers, gust loads and landing loads if desired. To evaluate the results of a loads analysis, quantities such as the bending moment (M_x), torsional moment (M_y) or the shear force (F_z) can be plotted against each other to form a load envelope, which are important in dimensioning the aircraft and checking the capability of the structure to withstand the requirements of a mission. The resulting load envelopes can then be used as an indication if and what adjustments to the structure of the aircraft are necessary.

4. Preliminary structural design

The preliminary structure of the TU-Flex aircraft was designed using the different workflows described in Sections 2 and 3. The fuselage, tail and wings of the aircraft have a mass of 3.15 kg, 1.05 kg and 3.98 kg, respectively. The rest of the mass of the aircraft results from the internal systems. The current weight of the aircraft is around 20kg. The isolated analysis of the wing shows that they are able to display a wing tip displacement of 6.33% with respect to the half span in a 1g condition and 12.7% in the 2g condition without violating the strain requirements. Figure 9 shows the static response of the wing for the 1g load case. The design process used for for the wing design has been presented in [16].

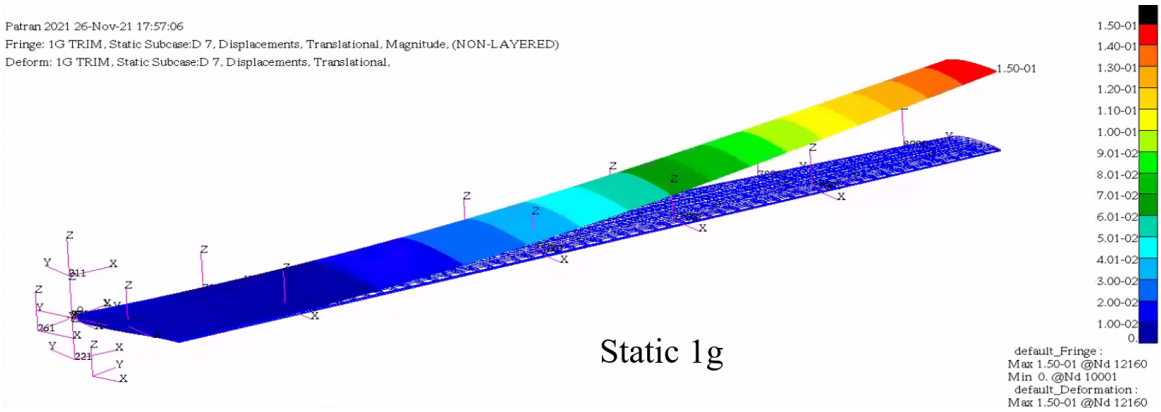

Figure 9 – Static response of the wing for 1g load case

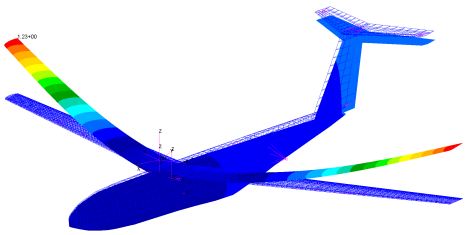

(a) Mode 1, 5.655 Hz, Symmetric first wing bending

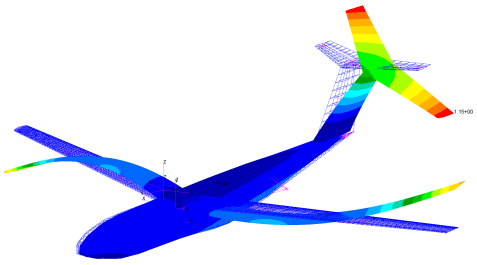

(b) Mode 2, 10.718 Hz, Asymmetric first wing bending & vertical stabilizer bending

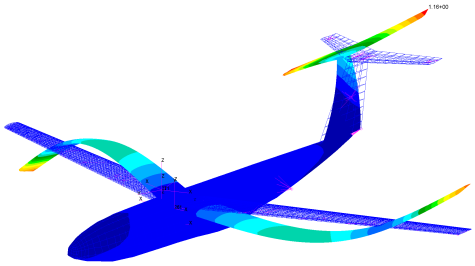

(c) Mode 3, 16.440 Hz, Asymmetric first wing bending & vertical stabilizer torsion

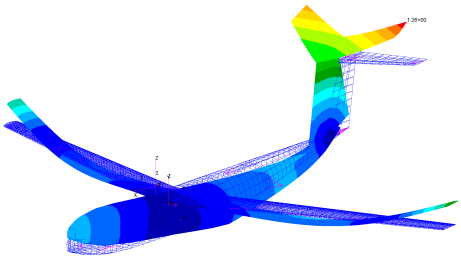

(d) Mode 4, 20.454 Hz, First fuselage bending

Figure 10 – First four normal mode shapes

Table 2 – First ten normal modes, frequencies and description of mode shape

Mode	Frequency [Hz]	Mode shape
1	5.655	Symmetric first wing bending
2	10.718	Asymmetric first wing bending and tail bending
3	16.440	Asymmetric first wing bending and tail torsion
4	20.454	First fuselage bending
5	23.845	Asymmetric first in-plane wing bending and tail bending
6	24.499	Symmetric second wing bending
7	29.738	Asymmetric second wing bending coupled with first in-plane wing bending and tail torsion
8	30.914	Asymmetric second wing bending coupled with first in-plane wing bending and tail torsion
9	32.013	Symmetric first in-plane wing bending
10	42.309	Asymmetric third wing bending and tail torsion

The normal modes of TU-Flex are of particular interest since a primary goal of the project is to investigate the coupling of structural modes and aircraft flight dynamics modes. The first ten normal modes, their frequencies and brief descriptions of the mode shapes are listed in Table 2. Figure 10 shows the first four normal mode shapes resulting from the SOL103 modal analysis in MSC.NASTRAN.

5. Load analysis

5.1 V-n diagram, flight path, performance

Figure 11 shows the flight envelope of TU-Flex. The load factor n ranges from +4 to -2, the flyable airspeed from 19 to 55 $\frac{m}{s}$ In the following load analysis the corner points of the flight envelope are of particular interest since the load on the structure is highest at those points. Thus the maneuvers for analysis are defined in such a way to reach the airspeed and load factor values from the flight envelope.

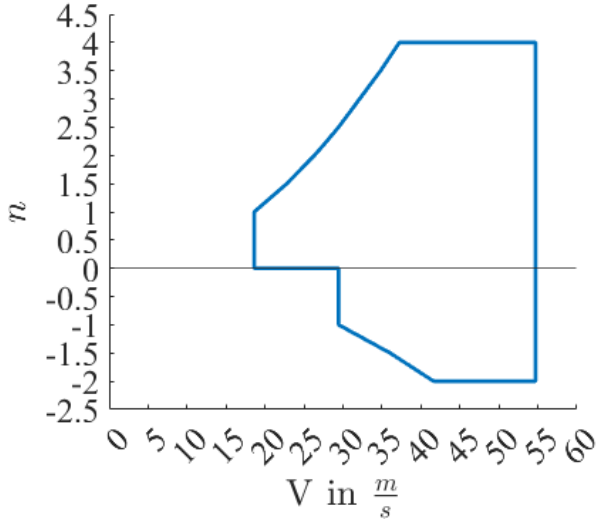

Figure 11 – Flight envelope of TU-Flex at sea level

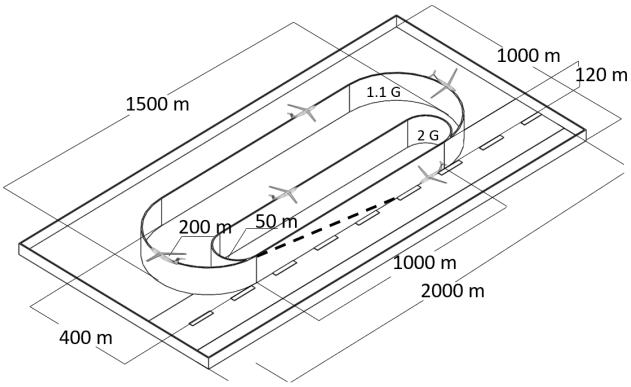

Figure 12 – Planned flight test profile

Additional considerations for the selection of maneuver cases were made. Load cases submitted for analysis were not only derived from the sizing load conditions but also from interesting flight conditions from the flight mechanics point of view, since the loads analysis also outputs the trim data for each load case. Thus flight mechanical considerations and comparisons can be made from the analysis as well. Interesting maneuvers can be determined using the illustration of the intended flight path in Fig. 12 and the performance diagrams in Fig. 13 to 16, including an assortment of pitching,

rolling, yawing, slip and roll- and pitch recovery maneuvers at different load factors.
Figure 13 shows the rate of climb and climb angle as a function of the airspeed. The highest rate of climb of $\approx 3.2\frac{m}{s}$ occurs at an airspeed of $V \approx 32\frac{m}{s}$. The largest climb angle $\Theta \approx 7.5°$ occurs at an airspeed of $V \approx 21\frac{m}{s}$. Figure 14 shows the turn radius and turn rate over the airspeed. Different turn maneuvers can be constructed from this data. Figures 15 and 16 show the maximum load factor for sustained level turn n and the maximum achievable bank angle ϕ as a function of the airspeed. These envelopes are constrained in their first section (dotted line) to the aerodynamic characteristics of the airplane (C_{Lmax}) and in the second section (continuous line) to the available thrust of the aircraft. Of particular interest are maximum load factor $n \approx 2.75$ and maximum bank angle $\phi \approx 70°$ during a sustained level turn, both of which occur at an airspeed of $V \approx 36.7\frac{m}{s}$.

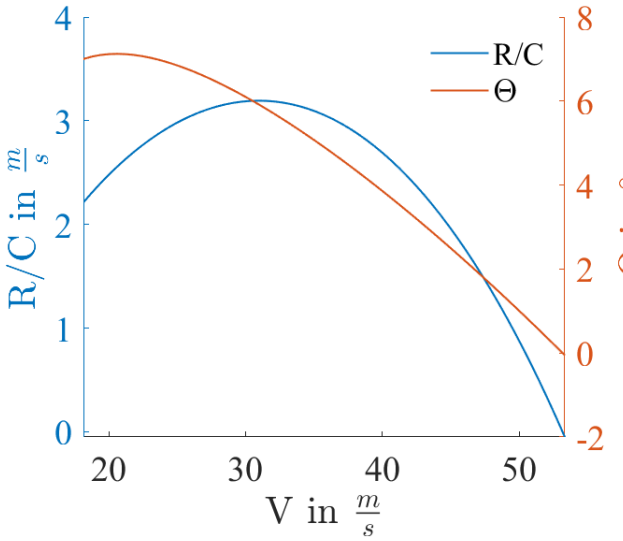

Figure 13 – Rate of climb and climb angle Θ over the airspeed V

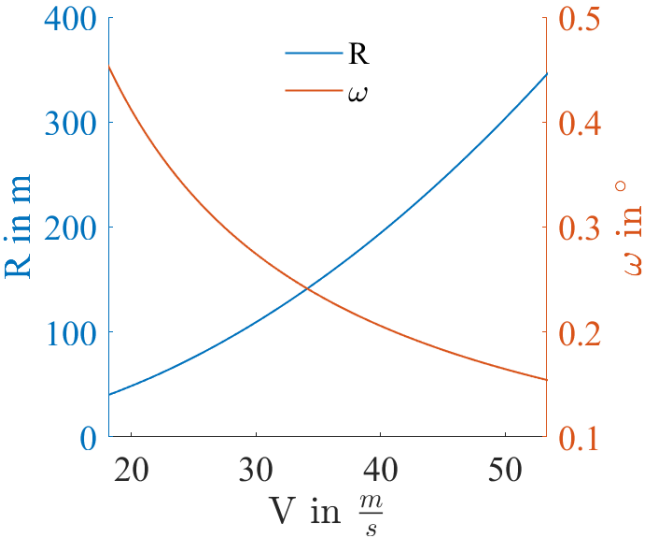

Figure 14 – Turn radius R and rate ω for $\phi = 40°$ over the airspeed V

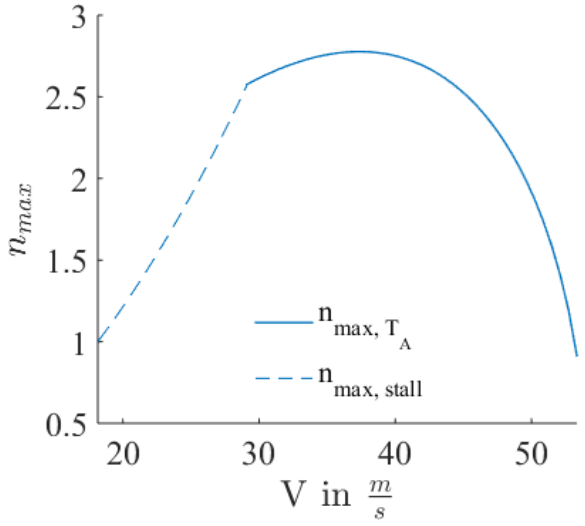

Figure 15 – Maximum load factor n during a sustained level turn over the airspeed V

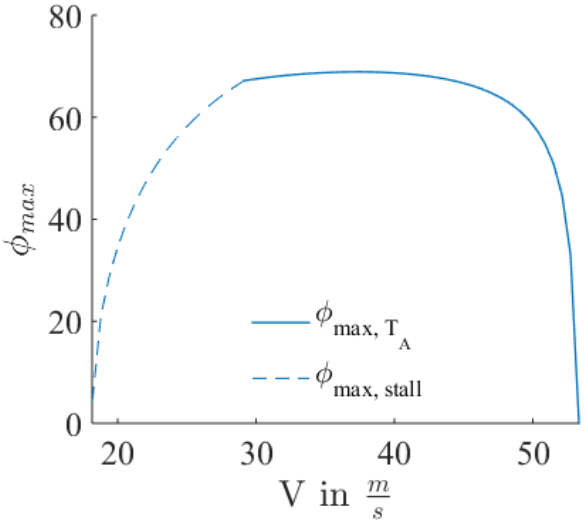

Figure 16 – Maximum bank angle ϕ over the airspeed V

The resulting load cases selected for analysis are summarized in Table 3. They are a mixture of reasonable flight maneuvers expected to be encountered during a flight test and the extreme cases at the edges of the flight envelope. Note that this list is not exhaustive but a preliminary set of load cases that have been considered in this stage of design.

Table 3 – Load cases analysed with Loads Kernel

Subcase	Maneuver description	Load factor N_z	Other parameters
1	Level flight	1.0	
2	200m radius turn	1.1	$\Phi = 25°$, $V = 30.25\frac{m}{s}$
3	200m radius turn	1.15	$\Phi = 30°$, $V = 33.65\frac{m}{s}$
4	200m radius turn	1.305	$\Phi = 40°$, $V = 40.57\frac{m}{s}$
5	50m radius turn	1.55	$\Phi = 50°$, $V = 24.18\frac{m}{s}$
6	50m radius turn	2.0	$\Phi = 60°$, $V = 29.15\frac{m}{s}$
7	50m radius turn	2.92	$\Phi = 70°$, $V = 36.71\frac{m}{s}$
8	roll maneuver	1.0	$p = 30\frac{°}{s}$, $V = 40\frac{m}{s}$
9	roll maneuver	1.0	$p = 60\frac{°}{s}$, $V = 40\frac{m}{s}$
10	Pull-up maneuver	1.1	$q = 1.41\frac{°}{s}$, $V = 40\frac{m}{s}$
11	Pull-up maneuver	1.5	$q = 7.03\frac{°}{s}$, $V = 40\frac{m}{s}$
12	Pull-up maneuver	2.5	$q = 21.08\frac{°}{s}$, $V = 40\frac{m}{s}$
13	Pull-up maneuver	4.0	$q = 42.16\frac{°}{s}$, $V = 40\frac{m}{s}$
14	Pull-up maneuver	4.0	$q = 30.66\frac{°}{s}$, $V = 55\frac{m}{s}$
15	Pull-up maneuver	4.0	$q = 45.56\frac{°}{s}$, $V = 37\frac{m}{s}$
16	Push-down maneuver	0.5	$q = -7.03\frac{°}{s}$, $V = 40\frac{m}{s}$
17	Push-down maneuver	0.0	$q = -14.05\frac{°}{s}$, $V = 40\frac{m}{s}$
18	Push-down maneuver	-1.0	$q = -28.1\frac{°}{s}$, $V = 40\frac{m}{s}$
19	Push-down maneuver	-2.0	$q = -42.16\frac{°}{s}$, $V = 42\frac{m}{s}$
20	Push-down maneuver	-2.0	$q = -30.66\frac{°}{s}$, $V = 55\frac{m}{s}$
21	Push-down maneuver	-1.0	$q = -37.47\frac{°}{s}$, $V = 30\frac{m}{s}$
22	Ascent at max. rate of climb	0.992	$\Theta = 7°$, $V = 32\frac{m}{s}$
23	Ascent at max. climb angle	0.991	$\Theta = 7.5°$, $V = 21\frac{m}{s}$
24	Fixed control surfaces	1.0	$\delta_a = \delta_e = \delta_r = 25°$, $V = 40\frac{m}{s}$
25	Fixed control surfaces	2.0	$\delta_a = \delta_e = \delta_r = 25°$, $V = 40\frac{m}{s}$
26	Fixed control surfaces	4.0	$\delta_a = \delta_e = \delta_r = 25°$, $V = 40\frac{m}{s}$
27	Slip	1.0	$\beta = 20°$, $V = 40\frac{m}{s}$
28	Slip	1.0	$\beta = 20°$, $\delta_a = \delta_r = 10°$, $V = 40\frac{m}{s}$
29	Roll recovery	1.0	$p = 30\frac{°}{s}$, $\dot{p} = -60\frac{°}{s}$, $V = 40\frac{m}{s}$
30	Roll recovery	4.0	$p = 30\frac{°}{s}$, $\dot{p} = -60\frac{°}{s}$, $V = 40\frac{m}{s}$
31	Pitch recovery	1.0	$q = 30\frac{°}{s}$, $\dot{q} = -60\frac{°}{s}$, $V = 40\frac{m}{s}$
32	Pitch recovery	4.0	$q = 30\frac{°}{s}$, $\dot{q} = -60\frac{°}{s}$, $V = 40\frac{m}{s}$
33	Pitch recovery	-1.0	$q = -30.66\frac{°}{s}$, $\dot{q} = 61.3\frac{°}{s}$, $V = 40\frac{m}{s}$
34	Pitch recovery	-2.0	$q = -42.16\frac{°}{s}$, $\dot{q} = 84.32\frac{°}{s}$, $V = 42\frac{m}{s}$

All flight mechanics angles are defined in a right-handed front-right-down coordinate system. The control surface angles δ_a, δ_e, δ_r are defined such that a positive δ_a of the ailerons induces a roll to the right, a positive δ_e of the elevators pitches the nose upwards and a positive δ_r of the rudder yaws the plane to the left.

5.2 Monitoring stations and load envelopes

To evaluate the results and identify dimensioning load cases the load envelopes are created. These load envelopes describe the resulting load quantities (forces and moments) due to a maneuver at monitoring stations located at interesting locations on the structure. An overview of the monitoring stations is shown in Fig. 17.

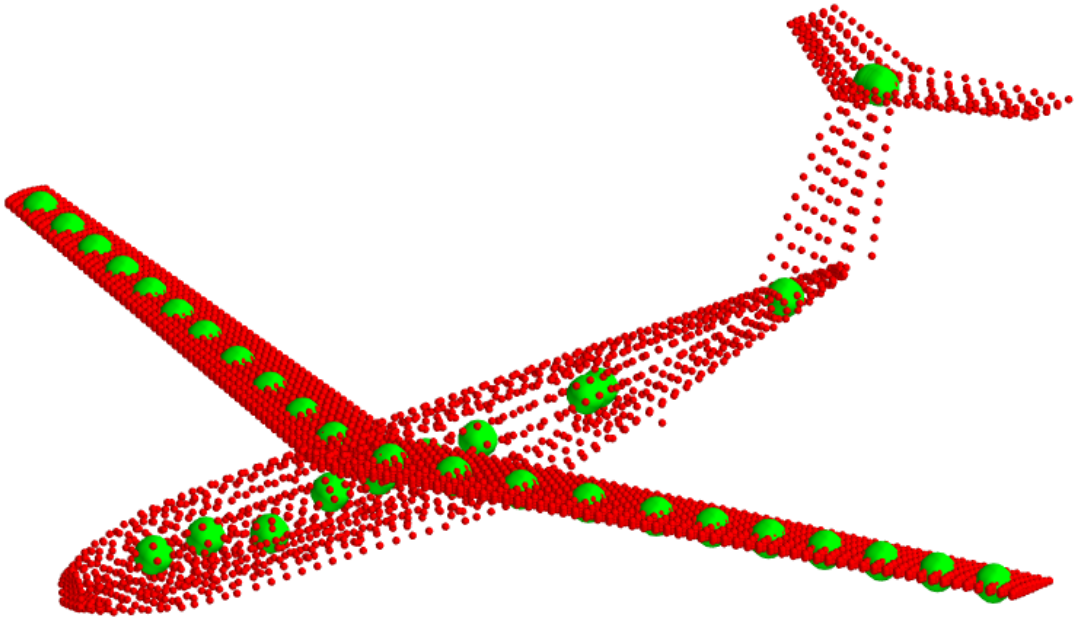

Figure 17 – Location of the monitoring stations

There are ten monitoring span wise along each wing to evaluate the shear force F_z, the bending moment M_x, and the torsional moment M_y along the wing during maneuvers. Nine monitoring stations are located along the fuselage at each frame in which the loads of the fuselage sections between frames are integrated. There are three monitoring stations in the tail assembly, one assigned to each horizontal stabilizer and one including the loads of the vertical stabilizer. A single monitoring station is located at the cargo floor of the aircraft. For each of these monitoring stations a load envelope is created for the following pairs of forces and moments:
F_z - M_x, M_x - M_y, F_z - M_y, F_y - M_x, M_x - M_z and M_y - M_z
Not all of these load combinations are equally useful for dimensioning the aircraft so special care has to be taken when identifying dimensioning load cases from the load envelopes. A particularly useful load envelope for example is the combination of shear force and bending moment F_z - M_x at the wing root.
Figure 18 shows a plot of the shear force F_z and the bending moment M_x integrated at a monitoring station located at the right wing root. The corner points of convex hull mark the dimensioning load cases. Figure 19 shows the shear force F_z and the torsional moment M_y at the connection between the vertical stabilizer and the horizontal stabilizer. Figures 20 and 21 show the shear and bending moment along the wingspan for all load cases. The curves with the highest values belong to dimensioning load cases, in this case load cases 14 and 19, vertical maneuvers at high load factors. Both load cases can also be identified as dimensioning load cases in the load envelopes in figures 18 and 19.

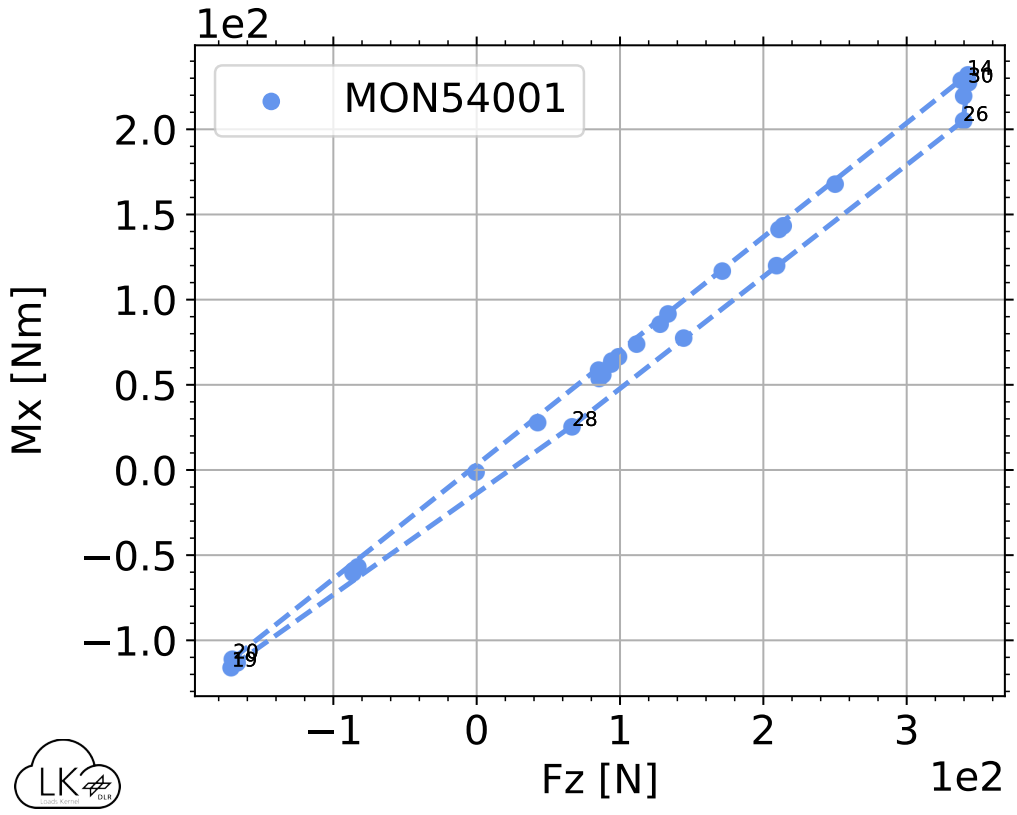

Figure 18 – Shear force F_z and bending moment M_x at the right wing root

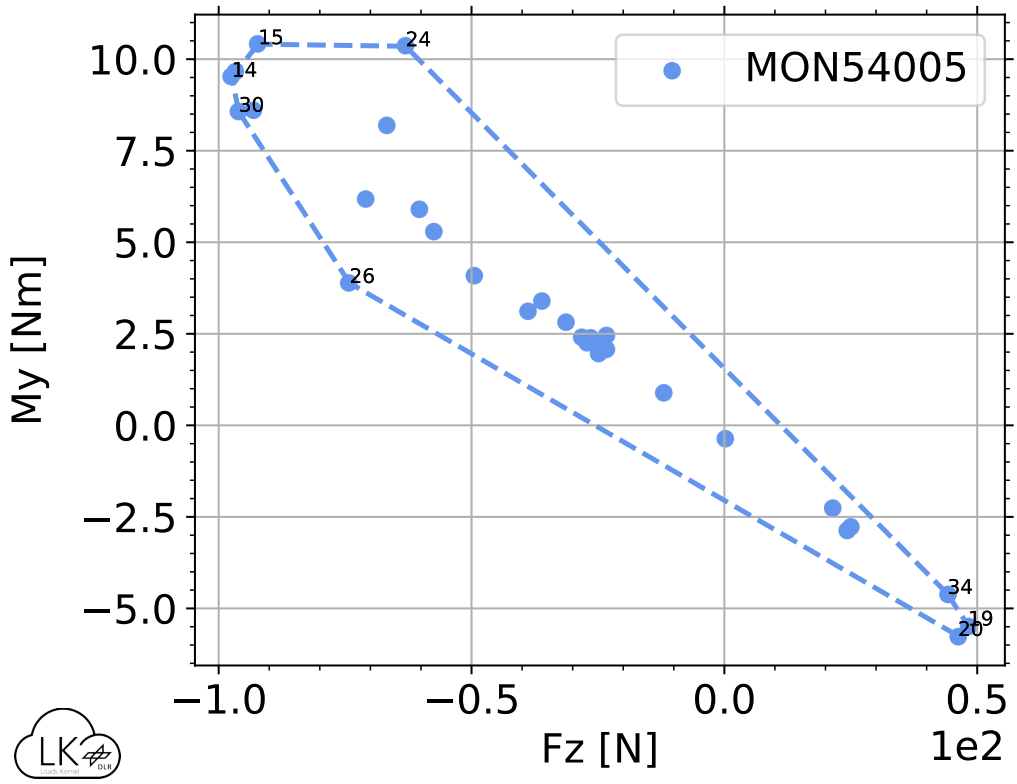

Figure 19 – Shear force F_z and torsional moment M_y at the intersection between vertical and horizontal stabilizers

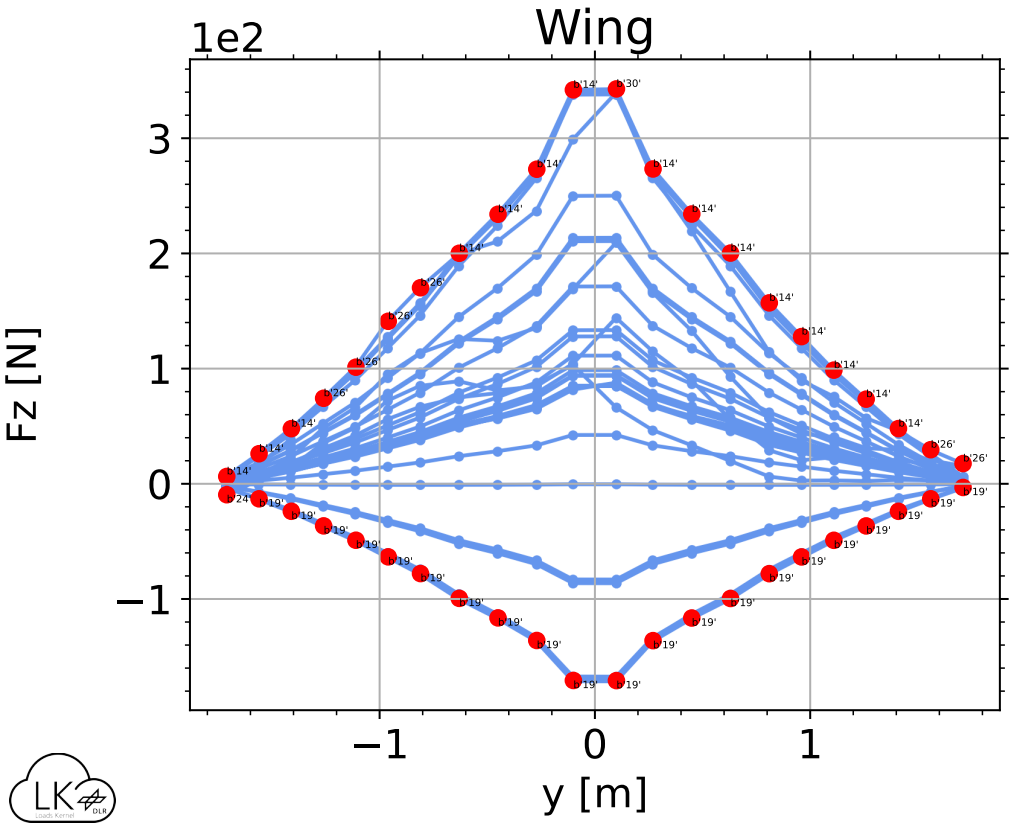

Figure 20 – Shear force F_z along the wingspan

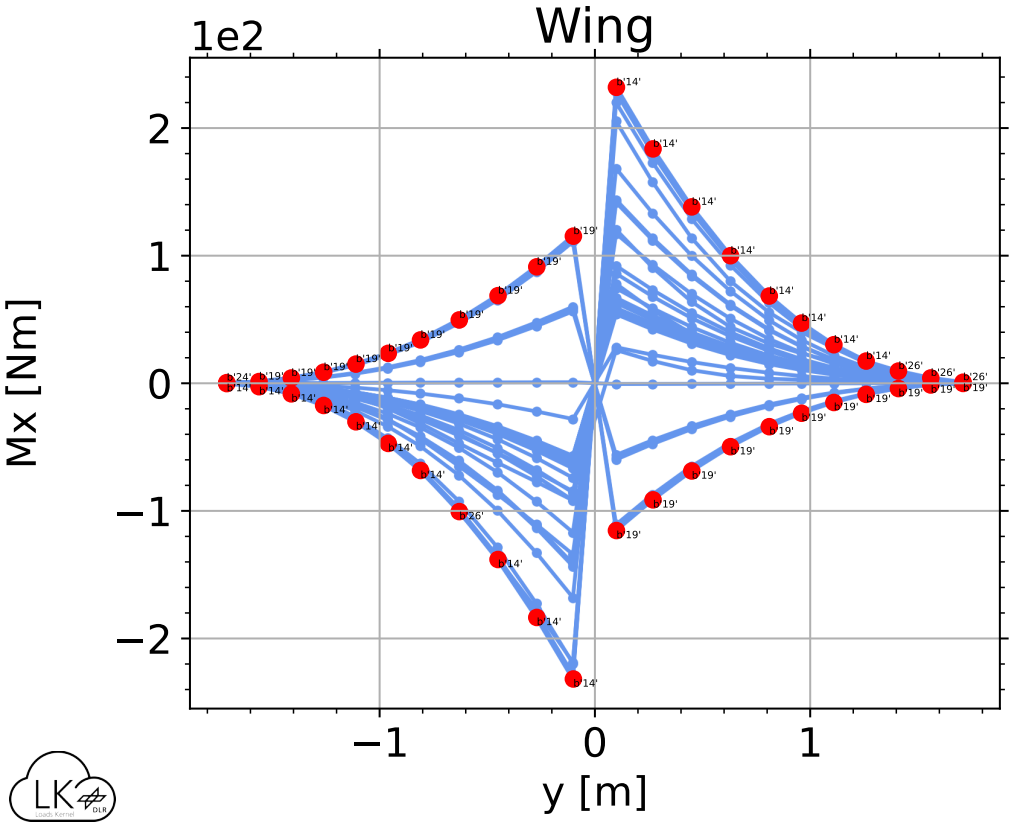

Figure 21 – Bending moment M_x along the wingspan

5.3 Strain analysis

To make the detailed evaluation of a load case possible, nodal loads (via FORCE and MOMENT NASTRAN cards) can be exported from the Loads Kernel analyis for each dimensioning load case. These can then be used in a NASTRAN SOL 101 linear static analysis to investigate the deformations and strains resulting from each load case and identify possible failure points and necessary adjustments to the structure. As a failure criterion a maximum allowable strain of $6000\frac{\mu m}{m}$ $(6 \cdot 10^{-}3\frac{m}{m})$ for the fuselage and $8000\frac{\mu m}{m}$ $(8 \cdot 10^{-}3\frac{m}{m})$ for the wings were set. Figure 22 shows the contour plots of the von-Mises strain tensor for equivalent homogeneous shell elements for two of the dimensioning load cases, 14 and 19. The plots were generated in PATRAN.
The largest strain with a value of $2.35 \cdot 10^{-3}\frac{m}{m}$ occurs in load case 14, the 4g pull-up maneuver at an airspeed of $55\frac{m}{s}$. This load case is located at the upper right corner of the flight envelope. The highest strain occurs at the wing roots. Notably the strain value is less than half of the allowable $6000\frac{\mu m}{m}$ for the fuselage and less than 30% of the $8000\frac{\mu m}{m}$ allowed for the wings. The highest deformation of the structure occurs in the same load case with the wing tips showing a deflection of 24.9 cm or 13.83 % with respect to the half span. Load case 19 shows the highest downwards deformation of the wing tips with a displacement of 12.4 cm or 6.9% with respect to the half span. The strains and deformations during all other load cases are lower than the ones in load case 14.

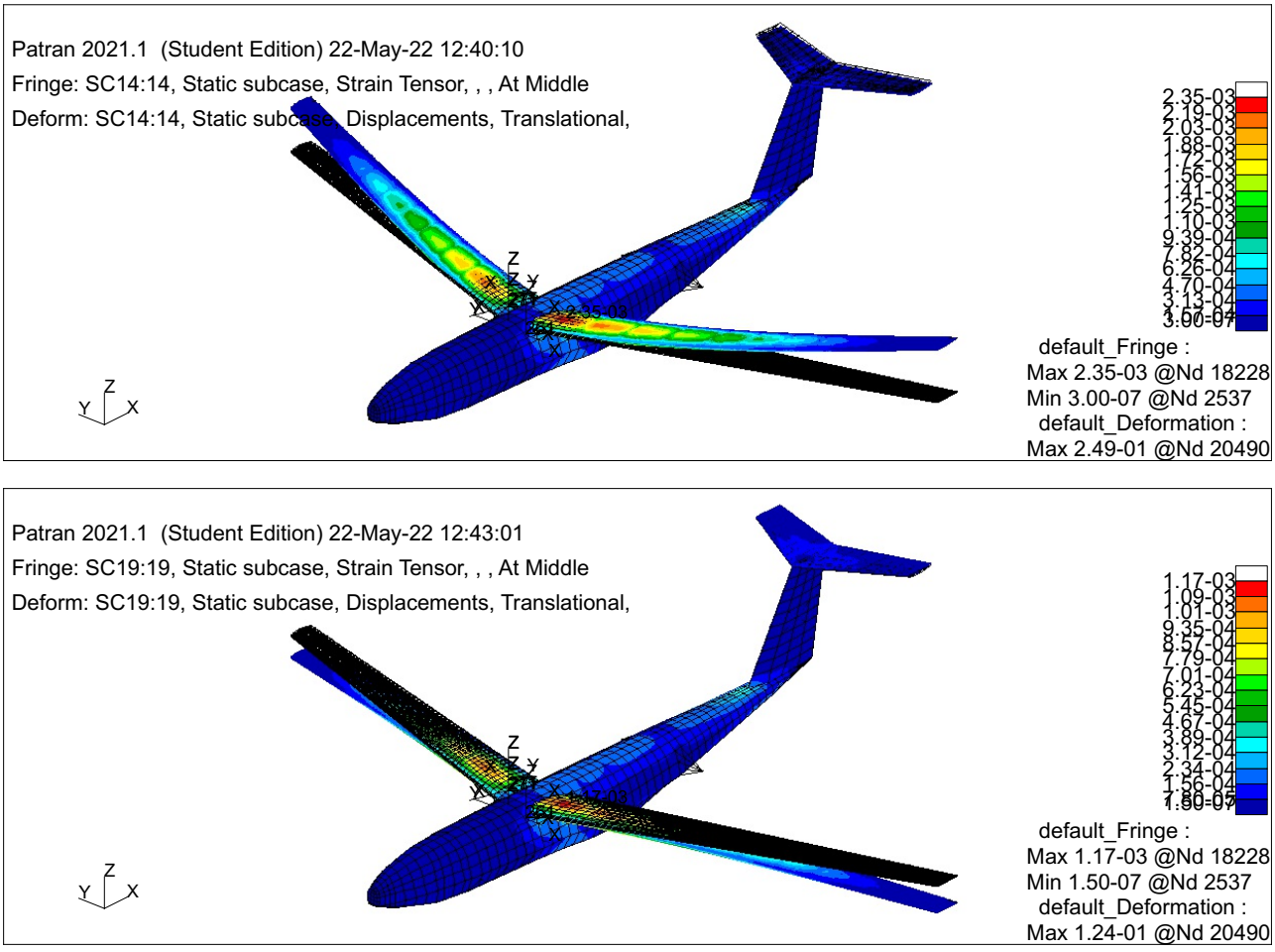

Figure 22 – Resulting strains on deformed geometry for load cases 14 and 19

6. Summary and outlook

This paper describes the preliminary structural design process of a flexible flying demonstrator. The design procedure started from a list of operational and feasibility requirements while considering geometrical, performance, sensors layout and facilities restrictions. Different methodologies were developed and applied to design the structure of this unconventional aircraft. The fuselage and wings' structural and aeroelastic models were generated and optimized according to specified load, deformation, mass and performance requirements. Finally, a full load analysis was performed to verify the integrity of the structural design.

The process started with OpenVSP draft. Then a CAD model was generated from this geometry. This CAD model provided the basis for the structural FE-model of the fuselage and tail assembly which were created in HyperMesh. The same software was used to generate the aerodynamic panel mesh of the demonstrator. The FE-model for the wing resulted from a optimization process using the DLR's software ModGen. Both structural models were then merged in HyperMesh. The aeroelastic model resulting from the structural and aerodynamic meshes could then be subjected to a loads analysis in the Loads Kernel software. The resulting load envelopes enabled the identification of dimensioning load cases which could then be analysed in detail using a NASTRAN SOL101 linear static analysis.

The procedures described in this work proved to be a comprehensive structural design process to generate models and carry out a load analysis. The combination of OpenVSP, CAD programs, HyperMesh, ModGen and Loads Kernel is particularly effective since most of the software is compatible with the NASTRAN format, allowing for the same files being used during the entire procedure, resulting in a streamlined process.

The preliminary load analysis of TU-Flex shows that for this configuration and selection of load cases, the structure is well within the bounds of allowable strains and deformations and appears feasible for construction and flight. Thus this design for the flexible wing configuration of TU-Flex will proceed to detailed design. The structural analysis process described here will be used further in the TU-Flex project, for the very flexible wing configuration.

7. Contact Author Email Address

The authors' contact e-mails are:p.gonzalez.ramirez@tu-berlin.de, gerrit.s.stavorinus@campus.tu-berlin.de, hikmat.shahi@dlr.de, muhammad.meddaikar@dlr.de, sunpeth.cumnuantip@dlr.de, arne.voss@dlr.de, thomas.klimmek@dlr.de, wolf.krueger@dlr.de and flavio.silvestre@tu-berlin.de.

8. Copyright Statement

References

[1] C. E. S. Cesnik, R. Palacios, and E. Y. Reichenbach, "Reexamined structural design procedures for very flexible aircraft," *Journal of Aircraft*, vol. 51, no. 5, pp. 1580–1591„ 2014.

[2] D. Drewiacki, F. J. Silvestre, and A. B. Guimarães Neto, "Influence of airframe flexibility on pilot-induced oscillations," *Journal of Guidance, Control, and Dynamics*, vol. 42, no. 7, pp. 1537–1550, 2019.

[3] A. B. Guimarães Neto, G. Barbosa, J. Paulino, R. Bertolin, J. Nunes, P. González, F. Cardoso-Ribeiro, M. Morales, R. da Silva, F. Bussamra, F. Silvestre, F. Moreira, and C. E. S. Cesnik, "Flexible aircraft simulation validation with flight test data," *AIAA Journal*, pp. 1–20, 2021.

[4] D. K. Schmidt, "Stability augmentation and active flutter suppression of a flexible flying-wing drone," *Journal of Guidance, Control, and Dynamics*, vol. 39, no. 3, pp. 409–422, 2016.

[5] C. Roessler, P. Stahl, F. Sendner, A. Hermanutz, S. Koeberle, J. Bartasevicius, V. Rozov, C. Breitsamter, M. Hornung, Y. Meddaikar, J. Dillinger, J. Sodja, R. De-Breuker, C. Koimtzoglou, D. Kotinis, and P. Georgopoulos, "Aircraft design and testing of flexop unmanned flying demonstrator to test load alleviation and flutter suppression of high aspect ratio flexible wings," in *Proceedings*, ser. AIAA 2019-1813, AIAA Scitech 2019 Forum. San Diego, California: AIAA, 2019.

[6] C. E. S. Cesnik, P. Senatore, W. Su, E. Atkins, and C. Shearer, "X-hale: A very flexible unmanned aerial vehicle for nonlinear aeroelastic tests," *AIAA journal*, vol. 50, no. 12, pp. 2820–2833, 2012.

[7] P. J. González, F. J. Silvestre, M. d. F. V. Pereira, Z. Y. Pang, and C. E. Cesnik, "Loop-separation control for very flexible aircraft," *AIAA Journal*, vol. 58, no. 9, pp. 3819–3834,, 2020.

[8] J. K. Dillinger, Y. M. Meddaikar, J. Lübker, M. Pusch, and T. Kier, "Design and optimization of an aeroservoelastic wind tunnel model," *Fluids*, vol. 5, no. 1, p. 35, 2020.

[9] T. Jordan, W. Langford, and J. Hill, "Airborne subscale transport aircraft research testbed-aircraft model development," in *AIAA Guidance, Navigation, and Control Conference and Exhibit*, 2005, p. 6432.

[10] P. Schmollgruber, J.-L. Gobert, P.-E. Gall, Z. Goraj, H. Jentink, A. Näs, and R. Voit-Nitchmann, "An innovative evaluation platform for new aircraft concepts," *The Aeronautical Journal*, vol. 114, no. 1157, pp. 451–456, 2010.

[11] "Openvsp," http://openvsp.org/, retrieved on: June 1, 2022.

[12] "Blender," https://www.blender.org/, retrieved on: June 1, 2022.

[13] "Hypermesh," https://www.altair.com/, retrieved on: June 1, 2022.

[14] T. Klimmek, "Parametric set-up of a structural model for fermat configuration aeroelastic and loads analysis," *Journal of Aeroelasticity and Structural Dynamics*, vol. 3, no. 2, 2014.

[15] ——, "Parameterization of topology and geometry for the multidisciplinary optimization of wing structures," in *CEAS 2009 - European Air and Space Conference*, 2009. [Online]. Available: https://elib.dlr.de/65746/

[16] P. J. González, H. Shahi, Y. M. Meddaikar, W. R. Krüger, and F. J. Silvestre, "Flexible-wing design process for tu-flex demonstrator," in *IFASD 2022 - International Forum on Aeroelasticity and Structural Dynamics, Madrid (accepted)*, 2022.

[17] A. Voß, "Design and structural optimization of a flying wing of low aspect ratio based on flight loads," Doctoral Thesis, Technische Universität Berlin, Berlin, 2020. [Online]. Available: http://dx.doi.org/10.14279/depositonce-9858

[18] ——, "An implementation of the vortex lattice and the doublet lattice method," German Aerospace Center (DLR), Tech. Rep. DLR-IB-AE-GO-2020-137, October 2020, https://elib.dlr.de/136536/.

[19] J. Katz and A. Plotkin, *Low-speed aerodynamics: From wing theory to panel methods*. McGraw-Hill, 1991.

[20] E. Albano and W. P. Rodden, "A doublet-lattice method for calculating lift distributions on oscillating surfaces in subsonic flows." *AIAA Journal*, vol. 7, no. 2, pp. 279–285, February 1969.